THREE-DIMENSIONAL OPTIMISATION OF A FUEL GAS CHANNEL OF A PEM FUEL CELL FOR MAXIMUM CURRENT DENSITY

S. O. Obayopo, T. Bello-Ochende*,† and J. P. Meyer

Department of Mechanical and Aeronautical Engineering, University of Pretoria, Pretoria, Private Bag X20, Hatfield, 0028, South Africa.

SUMMARY

Proton exchange membrane (PEM) fuel cells operated with hydrogen and air offer promising alternative to conventional fossil fuel sources for transport and stationary applications due to its high efficiency, low-temperature operation, high power density, fast start-up and potable power for mobile application. Power levels derivable from this class of fuel cell depend on the operating parameters. In this study, a three-dimensional numerical optimisation of the effect of operating and design parameters of PEM fuel cell performance was developed. The model computational domain includes an anode flow channel, membrane electrode assembly (MEA) and a cathode flow channel. The continuity, momentum, energy, and species conservation equations describing the flow and species transport of the gas mixture in the coupled gas channels and the electrodes were numerically solved using a computational fluid dynamics (CFD) code. The effects of several key parameters, including channel geometries (width and depth), flow orientation and gas diffusion layer (GDL) porosity on performance and species distribution in a typical fuel cell system have been studied. Numerical results of the effect of flow rate and gas diffusion layer porosity on the flow channel optimal configurations for PEM fuel cell are reported. Simulations were done ranging from 0.6 to 1.6 mm for channel width, 0.5 to 3.0 mm for channel depth and 0.1 to 0.7 for the GDL porosity. Results were evaluated at 0.3 V operating cell voltage of the PEM fuel cell. The optimisation results show that the optimum dimension values for channel depth and channel width are 2.0 and 1.2 mm, respectively. In addition, the results indicate that effective design of fuel gas channel in combination with the reactant species flow rate and GDL porosity enhances the performance of the fuel cell. The numerical results computed agree well with experimental data in the literature. Consequently, the results obtained provide useful information for improving the design of fuel cells.

KEY WORDS
Proton exchange membrane; fuel cells; computational fluid dynamics; optimisation; geometry; gas diffusion layer; flow orientation; optimal performance

Correspondence
*Tunde Bello-Ochende, Department of Mechanical and Aeronautical Engineering, University of Pretoria, Pretoria, Private Bag X20, Hatfield, 0028, South Africa.
†E-mail: Tunde.Bello-Ochende@up.ac.za

Contract/grant sponsor: National Research Foundation of the Republic of South Africa.

1. INTRODUCTION

Fuel cell technology is rapidly advancing due to the need for high energy efficiency and low environmental impact. Fuel cells are regarded as a potential reliable future source of energy supply due to the fact that they are one of the cleanest and most efficient alternatives for generating power. However, the large initial capital costs of fuel cell technology have offset the advantages it offers and slowed down its adoption for widespread applications [1,2]. Proton exchange membrane fuel cells (PEMFCs) using hydrogen are some of the emerging fuel cells with many advantages ranging from emission of water as waste, operation at low temperatures for quick start-up, and use of solid polymers as electrolytes, reducing both construction and safety complications [3-5]. This fuel cell type is seriously being considered as an alternative power source for stationary and mobile applications but there are several technical challenges which have to be overcome before it can be adopted for use in these devices.

One of the means of reducing the cost of PEMFCs is by improving their performance through system optimisation. This facilitates the understanding of how different parameters affect the performance of the fuel cell in real operating conditions and subsequently reduce the cost involved in prototype development. Fuel cell modeling has received tremendous attention in the last two decades with the ultimate aim of better understanding the underlying phenomenon of operating fuel cells.

Much research has been carried out on PEMFCs ranging from one-dimensional models showing phenomena where mass transport limitation is taken into

account and two or three-dimensional models encompassing thermal and water management. This two- or three-dimensional model also combines electrochemical, thermodynamic and fluid dynamic equations. Heat transfer equations and mass and energy balances were also incorporated into some studies to provide detailed understanding of emerging processes in fuel cell systems. In the landmark works on PEMFC by Bernardi [6], Bernardi and Verbrugge [7] and Springer *et al.* [8], which are based on one-dimensional models, the focus is on humidification requirements of inlet gases and issues related to variable membrane humidification. The work by this group [6-8] provided the required framework for the multidimensional models that followed in subsequent years.

A vast number of previous works are also CFD based. More recent works that are CFD based can be found in [9-23]. Available experimental work to date has been conducted mostly to validate highly sophisticated CFD simulations against the cell global polarisation curves. Some of the experimental studies can be found in [24-28].

Another issue of significant importance in PEM fuel cells is the pressure drop, especially at the cathode side of the cell. The product water generated at the cathode channel must be removed from the cell and this requires a high pressure drop. Also, too high pressure drops creates excessive parasitic power requirement for the pumping of air through the cells. Hence, the effective design of the fuel channel is required to ensure a balance in pressure drop requirements at the fuel cell cathode section.

Inoue *et al.* [29] studied gas flow through the GDL and the internal phenomena of a PEMFC single cell. The result shows an increase in flow when the differential pressure between adjoining channels is increased and the output density increases as the depth of the separator channel become smaller.

Liu *et al.* [30] studied two-phase flow and water flooding of reactants in the cathode flow channels of an operating transparent PEMFC experimentally. The effect of flow field type, cell temperature, cathode flow rate and operation time on water build-up and cell performance was studied. The results indicate the adverse effect of liquid water accumulation on mass transport and the subsequent reduction of the performance of the fuel cell.

Rodatz *et al.* [31] conducted studies on the operational aspects of a PEMFC stack under practical conditions. Their study focused particularly on the pressure

drop, two-phase flow and effect of bends. They observed a decrease in the pressure drops at a reduced stack current.

Maharudrayya *et al.* [32] studied the pressure drop and flow distribution in multiple parallel channel configurations used in PEMFC stacks. Through their study, they developed an algorithm to calculate the flow distribution and pressure drop in multiple U- and Z-type flow configurations of fuel cell.

Ahmed *et al.* [33] performed a numerical model to investigate the performance of PEMFC at high operating current densities for various channel cross-sectional configurations while maintaining the same reactant flow rates and inlet boundary conditions. The results obtained reveals that rectangular channel cross-sections gave higher cell voltages, but the trapezoidal channel cross-section gave more uniform distributions at the membrane-cathode GDL interface. Their result further reveals the presence of an optimum channel-shoulder ratio for optimal fuel cell performance.

Most of the existing models in the literature address the effect of fuel channel geometric parameters on the performance of the PEM fuel cell without investigating the mutual interdependence of the GDL porous medium, reactant gas flow rate and gas channel geometry on the fuel cell system performance. Studies on PEM fuel cell performances, which incorporate the determination of optimal operating values for fuel cell design parameters taking into consideration the combined mutual effect of channel geometry, flow rate, and GDL characteristics, are still very limited in the literature. A good understanding of the interactive interdependence of these fuel cell parameters is therefore essential for optimum fuel cell design. One crucial design consideration in fuel cell design is reactant flow in the flow field because of the dominant effect of the parasitic losses caused by frictional losses, reactant consumption, species production and blockages resulting from two-phase flow.

Therefore, the purpose of this study was to investigate the effect of a range of operating conditions such as reactant flow rates, GDL porosity, channel geometry and flow orientation on the performance of a single PEM fuel cell and also to determine the optimal operating conditions for this class of fuel cell. In addition, this study sought to determine the optimal fuel cell performance at different geometric configurations for a given gas diffusion layer porosity and reactant species flow rate, which has not been given much attention in the literature. In this paper, a three-dimensional steady-state computational model for a single PEM fuel cells was developed to predict the fuel cell performance under different operating conditions

and subsequently add to the knowledge base needed to produce generic design information for fuel cell systems, which can be applied to better designs of fuel cell stacks.

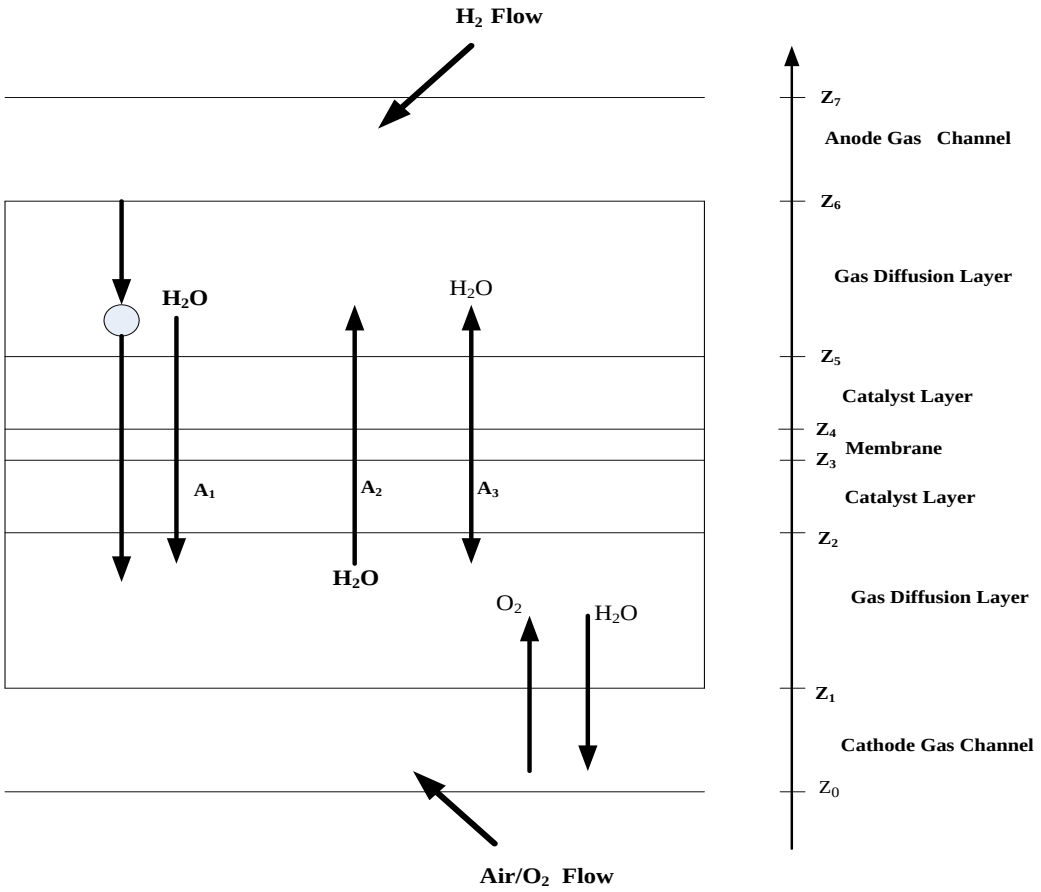

Figure 1 Schematic diagram of a PEM fuel cell showing different zones and species transport across the zones. The net water flux is the sum of: (A_1) electro-osmotic effect, (A_2) diffusion effect and (A_3) the permeability effect.

2. MODEL DESCRIPTION

Figure 1 shows a schematic diagram of a typical PEM fuel cell cross-section showing different zones and species transport across the zones. This consists of seven different regions: the cathode flow channel, cathode diffusion layer, cathode catalyst layer, proton exchange membrane, anode catalyst layer, anode diffusion layer, and the anode flow channel. It was assumed that the fuel is hydrogen at the anode side and diffuses through the porous gas diffusion layers and comes into contact with the catalyst layer. At this layer, it forms hydrogen ions and electrons. The hydrogen ion diffuses through the polymer electrolyte membrane at the centre while the electrons flow through the

gas diffusion layer to the current collectors and into the electric load attached. The electrochemical reactions are:

anodic: $H_2 \rightarrow 2H^+ + 2e^-$ (1)

cathodic: $\frac{1}{2}O_2 + 2H^+ + 2e^- \rightarrow H_2O$ (2)

net reaction: $H_2 + \frac{1}{2}O_2 \rightarrow H_2O$ (3)

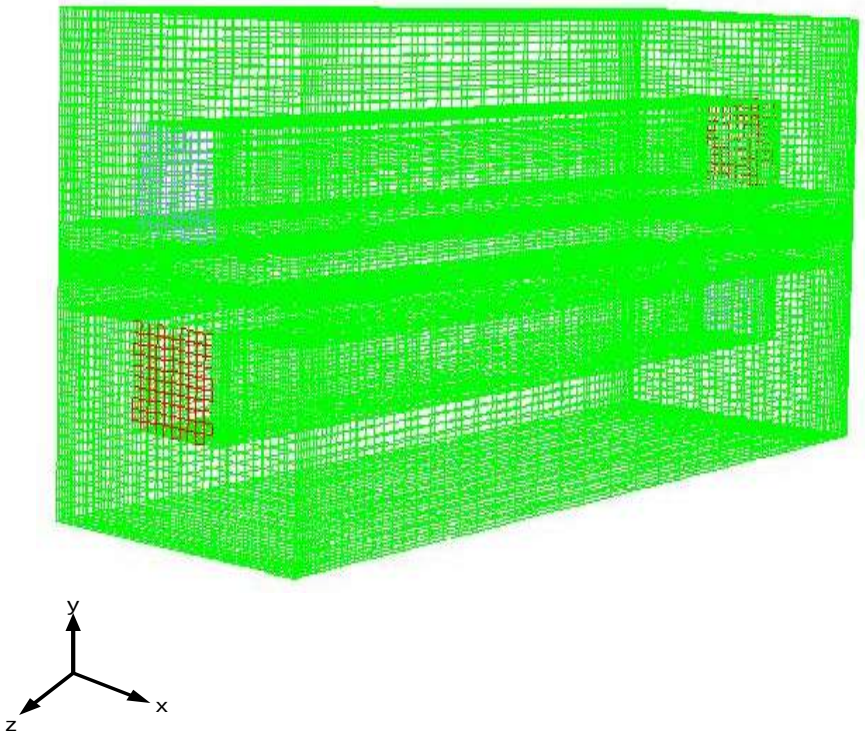

Figure 2 The discretised three-dimensional computational domain of a single PEM fuel cell.

Figure 2 depicts the computational domain consisting of the anode flow channel, anode diffusion layer, MEA assembly, cathode diffusion layer, and cathode flow channel. In this model, the numerical domain is a full single-cell geometry domain. Pure hydrogen and air were used as reactant gases in the model. The inlet flow velocity was controlled by stochiometry numbers of 1.2 at the anode and 2.0 at the cathode. The operating pressure was 101 kPa absolute at the exit of the cell. The details of the flow field and other physicochemical parameters used for the base case are summarised in Table 1 and Table 2.

Table I. Base case geometric parameters of the modeled fuel cell

Channel length (mm)	120
Channel width (mm)	1.0
Channel depth (mm)	1.2
Membrane thickness (mm)	0.036
Catalyst layer thickness (mm)	0.012
Electrode thickness (mm)	0.21

Table II. Physicochemical properties of the modeled fuel cell

Description	Value	References
Cell operating temperature (^{o}C)	70	[3,23]
Air-side/fuel-side inlet pressure (atm)	3/3	[35]
Open-circuit voltage (V)	0.95	[35]
Porosity of gas diffuser layer	0.4	[21,28,38]
Permeability of gas diffuser layer (m^2)	1.76×10^{-11}	[21,28,38]
Tortuosity of gas diffuser layer	1.5	[37,16]
Porosity of catalyst layer	0.4	[21,22,28]
Permeability of catalyst layer (m^2)	1.76×10^{-11}	[16, 21,28]
Tortuosity of catalyst layer	1.5	[16,37]
Porosity of membrane	0.28	[16,21,28]
Permeability of membrane (m^2)	1.8×10^{-18}	[16,21,28]
Reference diffusivity of H_2	11×10^{-5} m^2 s^{-1}	[14]
Reference diffusivity of O_2	3.2×10^{-5} m^2 s^{-1}	[14]
Electric conductivity of catalyst layer $(\Omega^{-1}m^{-1})$	190	[47]
Electric conductivity of GDL $(\Omega^{-1}m^{-1})$	300	[34]
Electric conductivity in carbon plate $(\Omega^{-1}m^{-1})$	4000	[34,47]
O_2 stochiometry ratio	1.2	[35]
H_2 stochiometry ratio	2.0	[22,35]
Oxygen mole fraction	0.406	[35]
Relative humidity of inlet fuel/air	100%	[3]
Reference current density of anode (A/m^2)	7 500	[35]
Reference current density of cathode (A/m^2)	20	[35]
Anode transfer coefficient	2.0	[35]
Cathode transfer coefficient	2.0	[35]

2.1 Model assumptions

In the modelling of the fuel cell the following assumptions were made: the cell operates under steady-state conditions, isothermal boundary conditions were used for external walls, the flow in the cell is considered to be laminar, reactant and products

are assumed to be ideal gas mixtures, and the electrode is assumed to be an isotropic and homogeneous porous medium.

2.2 Governing transport equations

The basic transport equation (conservation of mass and momentum) applies to the transport of gas mixtures in the gas channels in the fuel cell. The corresponding governing equations are written as follows:

Continuity equation,

$$\frac{\partial(\rho v_x)}{\partial x} + \frac{\partial(\rho v_y)}{\partial y} + \frac{\partial(\rho v_z)}{\partial z} = S_m \tag{4}$$

S_m is the source term due to electrochemical reactions corresponding to the hydrogen depletion during reactions, which is applicable at both the anode and cathode GDL/MEA interface and is given by [15]:

$$S_m = 0, \qquad z_0 \le z \le z_2 \tag{5}$$

$$S_m = -\frac{\lambda[H_2]}{\kappa + [H_2]}, \qquad z_2 \le z \le z_3 \tag{6}$$

Where $[H_2]$ is the concentration of hydrogen in the domain of interest and λ and κ are terms whose values are dependent upon the rate constants for the atomic oxidation of H_2 and the platinum loading in the catalyst layer. The value of κ was set equal to 1 and λ assumed different values, which were subject to different values of the concentration of platinum initially in the catalyst layer as discussed by Hontanon *et al*. [15]. The momentum conservation, also referred to as Navier-Stokes equation, is:

Momentum (*x*- direction):

$$v_x \frac{\partial(\rho v_x)}{\partial x} + v_y \frac{\partial(\rho v_x)}{\partial y} + v_z \frac{\partial(\rho v_x)}{\partial z}$$

$$= -\frac{\partial P}{\partial x} + \frac{\partial}{\partial x}\left(\mu \frac{\partial v_x}{\partial x}\right) + \frac{\partial}{\partial y}\left(\mu \frac{\partial v_x}{\partial y}\right) + \frac{\partial}{\partial z}\left(\mu \frac{\partial v_x}{\partial z}\right) + S_{px} \tag{7}$$

Momentum (*y*- direction):

$$v_x \frac{\partial(\rho v_y)}{\partial x} + v_y \frac{\partial(\rho v_y)}{\partial y} + v_z \frac{\partial(\rho v_y)}{\partial z}$$

$$= -\frac{\partial P}{\partial y} + \frac{\partial}{\partial x}\left(\mu \frac{\partial v_y}{\partial x}\right) + \frac{\partial}{\partial y}\left(\mu \frac{\partial v_y}{\partial y}\right) + \frac{\partial}{\partial z}\left(\mu \frac{\partial v_y}{\partial z}\right) + S_{py} \tag{8}$$

Momentum (*z*- direction):

$$v_x \frac{\partial(\rho v_z)}{\partial x} + v_y \frac{\partial(\rho v_z)}{\partial y} + v_z \frac{\partial(\rho v_z)}{\partial z}$$

$$= -\frac{\partial P}{\partial z} + \frac{\partial}{\partial x}\left(\mu \frac{\partial v_z}{\partial x}\right) + \frac{\partial}{\partial y}\left(\mu \frac{\partial v_z}{\partial y}\right) + \frac{\partial}{\partial z}\left(\mu \frac{\partial v_z}{\partial z}\right) + S_{pz} \tag{9}$$

The source terms account for situations when a fluid passes through a porous medium. In this paper, the term is applicable to the electrode and catalyst zones. For low velocities encountered in fuel cells, these source terms are applicable at the gas diffusion layers and are given by Darcy's law:

$$S_{px} = -\frac{\mu v_x}{\beta_x}; \tag{10}$$

$$S_{py} = -\frac{\mu v_y}{\beta_y}; \tag{11}$$

$$S_{pz} = -\frac{\mu v_z}{\beta_z}; \tag{12}$$

at $z_1 \le z \le z_6$

where μ is the fluid viscosity in the medium and β is the permeability of the electrode material. The permeability of the medium was assumed to be isotropic as stated in the assumptions in this model, hence β_x, β_y, and β_z all have the same value stated in Table 1 (1.76 x 10^{-11} m^2). Other source terms for the equations above used in the model were taken from Dutta *et al.* [13]. The local current density i_o is a measure of the electrochemical reaction rate and generally given by the Butler-Volmer equation [34]:

$$i_o = i_{o,ref}\left\{\exp\left[\frac{\alpha_{an} nF}{RT}\eta\right] - \exp\left[\frac{-\alpha_{cat} nF}{RT}\eta\right]\right\} \tag{13}$$

where η is the overpotential and defined as,

$$\eta = \left(\Phi_s - \Phi_e\right) - E_{ocv} \tag{14}$$

The energy conservation equation is:

$$\frac{\partial(\rho v_x h)}{\partial x} + \frac{\partial(\rho v_y h)}{\partial y} + \frac{\partial(\rho v_z h)}{\partial z} = \frac{\partial}{\partial x}\left(k\frac{\partial T}{\partial x}\right) + \frac{\partial}{\partial y}\left(k\frac{\partial T}{\partial y}\right) + \frac{\partial}{\partial z}\left(k\frac{\partial T}{\partial z}\right) + S_T \tag{15}$$

For the energy equation, additional volumetric sources are present because not all chemical energy released in the electrochemical reaction can be converted to electrical work due to irreversibilities of the process. The total source that goes to the thermal energy equation (i.e., enthalpy) is [35]:

$$S_h = h_{react} - R_{an,cat}\eta_{an,cat} + I^2 R_{ohm} + h_L \tag{16}$$

Proton exchange membrane fuel cells operate under relatively low temperature (< 100 ^oC), the water vapour may condense to liquid water, especially at high current densities. The existence of the liquid water keeps the membrane hydrated, but it also blocks the gas diffusion layer passage, reduces the diffusion rate and the effective reacting surface area. The water formation and transport of liquid water is modeled using a saturation model based on [36,37]. In this approach, the liquid water

formation and transport is governed by the conservation equation for the volume fraction of liquid water, *s*, or the water saturation [35]:

$$\frac{\partial(\epsilon\rho_l s)}{\partial t} + \nabla \cdot \left(\rho_l \vec{V_l} s\right) = r_w \tag{17}$$

where the subscript l represents liquid water, and r_w is the condensation rate modeled as,

$$r_w = c_r \max\left(\left[(1-s)\,\frac{P_{wv}-P_{sat}}{RT} M_{w,H_2O}\right], [-s\rho_l]\right) \tag{18}$$

where r_w is added to the water vapor equation, as well as the pressure correction (mass source). The condensation rate constant is hardwired to $c_r = 100s^{-1}$. It is assumed that the liquid velocity, V_l, is equivalent to the gas velocity inside the gas channel. Inside the highly-resistant porous zones, the use of the capillary diffusion term allows the replacement of the convective term in Equation (17):

$$\frac{\partial(\epsilon\rho_l s)}{\partial t} + \nabla \cdot \left[\rho_l \frac{Ks^3}{\mu_l}\frac{dp_c}{ds}\nabla s\right] = r_w \tag{19}$$

Depending on the wetting phase, the capillary pressure is computed as a function of *s* (the Leverett function) [35,38]:

$$p_c = \begin{cases} \dfrac{\sigma\cos\theta_c}{(\frac{K}{\varepsilon})^{0.5}}(1.417(1-s)-2.12(1-s)^2+1.263(1-s)^3, \theta_c<90^oC \\ \dfrac{\sigma\cos\theta_c}{(\frac{K}{\varepsilon})^{0.5}}(1.417s-2.12s^2+1.263s^3), \theta>90^oC \end{cases} \tag{20}$$

Equation (17) models various physical processes such as condensation, vaporisation, capillary diffusion, and surface tension. The clogging of the porous media and the flooding of the reaction surface are modeled by multiplying the porosity and the active surface area by (1- *s*), respectively.

2.3 Channel cross-section

Flow channels in fuel cells are typically rectangular in cross-section, though other configurations such as triangular, trapezoidal, and semi-circular have been explored for fuel cell designs [15]. The manufacturing processes of the flow channels in fuel cell are quite time-consuming and expensive since graphite, which is hard and brittle, is typically used as the material of choice. Hence the making of the flow channel is a major cost in the development of a complete PEM fuel cell. In the design of small fuel cells, where the pressure drop is of the order of 0.5-1 bar [39], serpentine or interdigitated channels could be applicable but in larger fuel cells, this is not possible as the pressure drop would be in the order of a few bars. From cost considerations and manufacturing and performance requirements, the geometrical shape of the channel cross-section has traditionally been either rectangular or square. The rectangular cross-section was used in the design of the PEM fuel cell in this study and is schematically shown in Figure 3.

For internal flows such as the ones in fuel cell channels, the Reynolds number is conventionally defined as [40]:

$$Re_{D_h} = \frac{\rho V_{avg} D_h}{\mu} \tag{21}$$

$$V_{avg} = \frac{\dot{m}}{\rho A_c} \tag{22}$$

For a rectangular channel in this study, D_h is defined as [40]:

$$D_h = \frac{4A_c}{P^*} \tag{23}$$

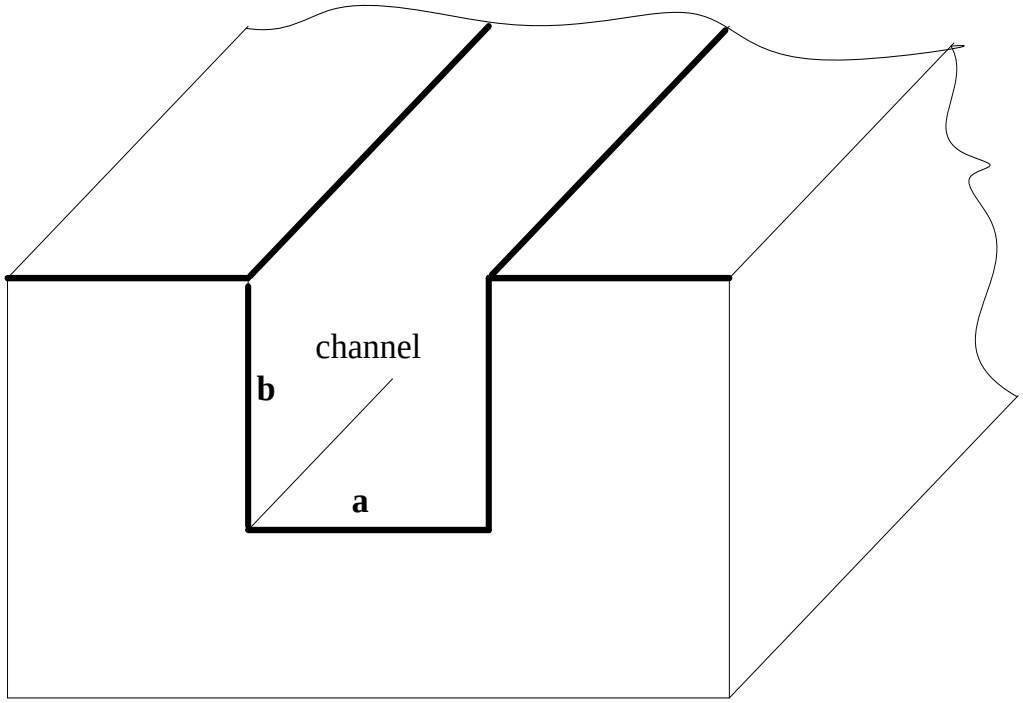

Figure 3 Channel cross-sectional view.

For the channel under consideration in Figure 3, the cross-sectional area is equal to the product of the channel width and the channel depth.

$$A_c = ab \tag{24}$$

and the wetted perimeter is

$$P^* = 2(a + b) \tag{25}$$

The pressure drop for a flow in a channel of length L is usually expressed using the following relation [40]:

$$\Delta p = f \frac{L}{D_h} \frac{\rho V_{avg}^2}{2} \tag{26}$$

where the friction factor f for steady fully developed laminar flows in a channel with square cross-section is given as

$$f = \frac{56.91}{Re_{D_h}} \tag{27}$$

Substituting the above relation Eq. (17) into Eq. (16), and taking into consideration Eqs. (11) to (15), the pressure drop can be obtained for flow channels with square cross-section (a = b), as

$$\Delta P = 28.455 \left(\frac{\mu \dot{m}}{\rho}\right)\left(\frac{L}{a^4}\right) \tag{28}$$

Thus the flow channel length for flow channels with a square cross-section can be determined as

$$L = \frac{\Delta p \rho a^4}{28.455 \mu \dot{m}} \tag{29}$$

Similarly, we can obtain the flow channel length for a rectangular cross-section as

$$L = \frac{8\Delta p \rho (ab)^3}{C \mu \dot{m} (a+b)^2} \tag{30}$$

where $C = fReD_h$ is a function of the b/a for rectangular flow channels [40].

The pressure drop in the channel can be obtained using the flow rate (q) − pressure drop ΔP relationship for a rectangular cross-section relation [41]:

$$q = \frac{4ba^3}{3\mu} \times \frac{-\Delta P}{\Delta L}\left[1 - \frac{192}{\pi^5 b}\sum_{i=1,3,5..}^{\infty} \frac{\tanh(i\pi b/2a}{i^5}\right] \tag{31}$$

2.4 Fluid flow through GDL

In fuel cells, the fluid flow diffuses through the GDL for the reaction to take place on the MEA. The effective diffusivity for gas-phase flow in porous media can be written as:

$$D_{eff} = D\frac{\varepsilon}{\tau} \tag{32}$$

The tortuosity (τ) is a difficult parameter to estimate except through experiment. Hence it is usually correlated in fuel cell studies using a Bruggeman correlation. This correlation assumes τ is proportional to $\varepsilon^{-0.5}$ resulting in the simpler expression [42]:

$$D_{eff} = D\varepsilon^{1.5} \tag{33}$$

The porosity correlation is used to adjust for the longer effective path length through the porous media.

2.5 Boundary conditions

Pressure boundary conditions were specified at the outlets since the reactant gas flow is usually separate and at different pressures. The inlets were all assigned as mass flow inlets. The gas diffusion layer and the catalyst layer were surrounded by sealed plates at the inlet and outlet planes, so the boundary conditions at the inlet and outlet planes take the no-slip condition for the velocity and non-permeable condition for the species mass fraction. The membrane-electrode interface was defined as a wall, primarily to inhibit species and electron crossover through the membrane. This also prevents pressure problems at the interface. In the areas at which the gas diffusion electrodes were in contact with the bipolar plates, a constant reference voltage equal to zero was assigned as a boundary condition both at the anode and at the cathode. The electron flux was set to zero at all other walls. The anode was grounded (V = 0) and the cathode terminal was set at a fixed potential (0.75 V) less than the open-circuit potential (0.95 V). Both anode and cathode terminals were assigned wall boundaries.

2.6 Solution technique

The model equations were solved using the CFD software ANSYS Fluent® 12.0 with Gambit® (2.4.6) as a pre-processor. The CFD code has an add-on package for fuel cells, which has the requirements of the source terms for species transport equations, heat sources and liquid water formations [35]. Control volume technique was used for solving the problem. The meshes were more refined at the membrane-

catalyst assembly regions. The conservation of mass, momentum and energy equations in the three-dimensions were solved, in turn, until the iterative process met the convergence criteria. In this study, the definition of convergence criteria indicates that the largest relative error between two consecutive iterative residuals within the overall computational domains is less that 10^{-6}.

Several works have been done towards development of metrics for validation and verification of the computational code used in fluid flow modeling. American Institute of Aeronautics and Astronautics (AIAA) and American Society of Mechanical Engineers (ASME) have also declared policy statements and guidelines for the verification and validation of computational fluid dynamics simulations [43, 44]. These metrics include assessment for iterative convergence, spatial grid convergence and comparison of the CFD results to experimental data. These criteria are used in this work.

The domain was divided into hexahedral volume elements. A computational mesh of about 257 346 volume elements was obtained with the grid. The grid independence was verified at the preliminary test runs. Four structured grid configurations were evaluated for the PEMFC. The number of elements in the *x*-, *y*-, and *z*- directions was: (a) 70 × 70 × 25, (b) 87 × 87 × 34, (c) 104 × 87 × 34 and (d) 104 × 104 × 43. The influence of the number of elements on the local current density at an operating voltage of 0.4 V was investigated. The local current density for grid (a) differs from that of (b-d) with deviation of about 4.2%. However, the local current density distributions for grids (b), (c) and (d) do not show any significant differences. The difference between the local current densities for (b) and (c) is about 0.36% and the difference between (c) and (d) is 0.48%. Grid (c) was chosen for the simulations as a trade-off between accuracy and cost of time.

The solution strategy was based on the SIMPLE algorithm [45]. Momentum equations were solved for the velocity followed by solving the equation of continuity, which updates the pressure and the flow rate. Results were then verified for convergence. The simulation for each operating potential converged in 45 - 60 minutes depending on the current density on an Intel® Core(TM) 2Duo 3.00 GHz PC with 3.24 GB of DDRam.

2.7 Model validation

The validation of physical and numerical models is very important; hence comparison with some experimental data is highly desirable. For fuel cell performance description, the polarisation curve or voltage-current curve is one of the most important final outcomes of numerical simulations and is widely used for validation purposes [46]. The simulation results for the base case operating conditions were verified against experimental measurements of Wang *et al.* [47] and Cheng *et al.* [34]. The computed polarisation curve shown in Figure 4 is in good agreement with the experimental curves in the low load region. However, the model current density in the high mass transport limited region (> 2.75 A/cm^2) is higher than the experimental values. This observation is common in models where the effect of reduced oxygen transport due to water flooding at the cathode at higher current density cannot be properly accounted for [48]. Nonetheless, the prediction from the model could still successfully be used for better understanding of the complicated processes in fuel cell systems.

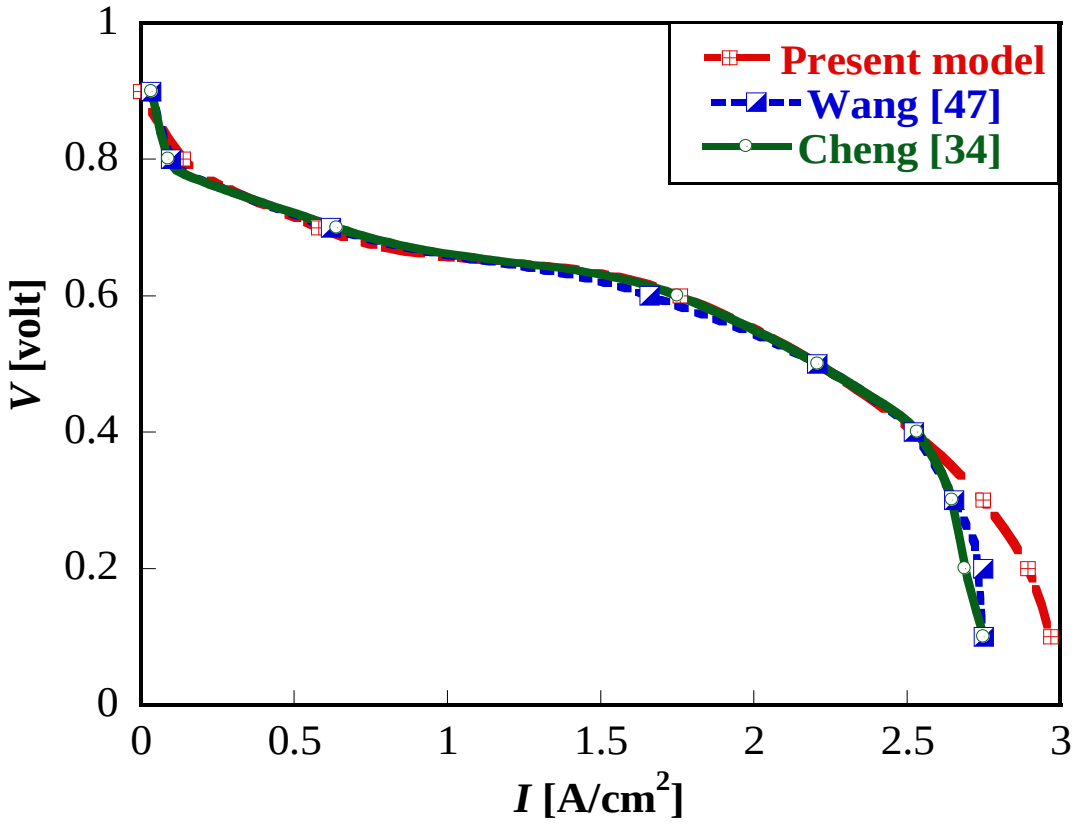

Figure 4 Comparison of numerical model prediction and experimental polarisation curves at base condition.

3. MODEL RESULTS AND DISCUSSION

3.1 Pressure drop in flow channel

Figure 5 shows the calculated pressure drops for the rectangular flow channel over a range of air mass flow rates at a channel depth and width of 1.2 mm and 1.0 mm, respectively. The results indicate that the pressure drop increases as the mass flow rate at the cathode is increased. This is expected since an increase in the mass flow rate increases the reaction of the reactant species and also reduces the resident water in the cathode channel of the fuel cell. Generally, fuel cells with high pressure drops in the flow field exhibit a more even distribution of the reactant species flow than those with low pressure drops in their flow fields. These even distributions do greatly enhance the fuel cell performance [49].

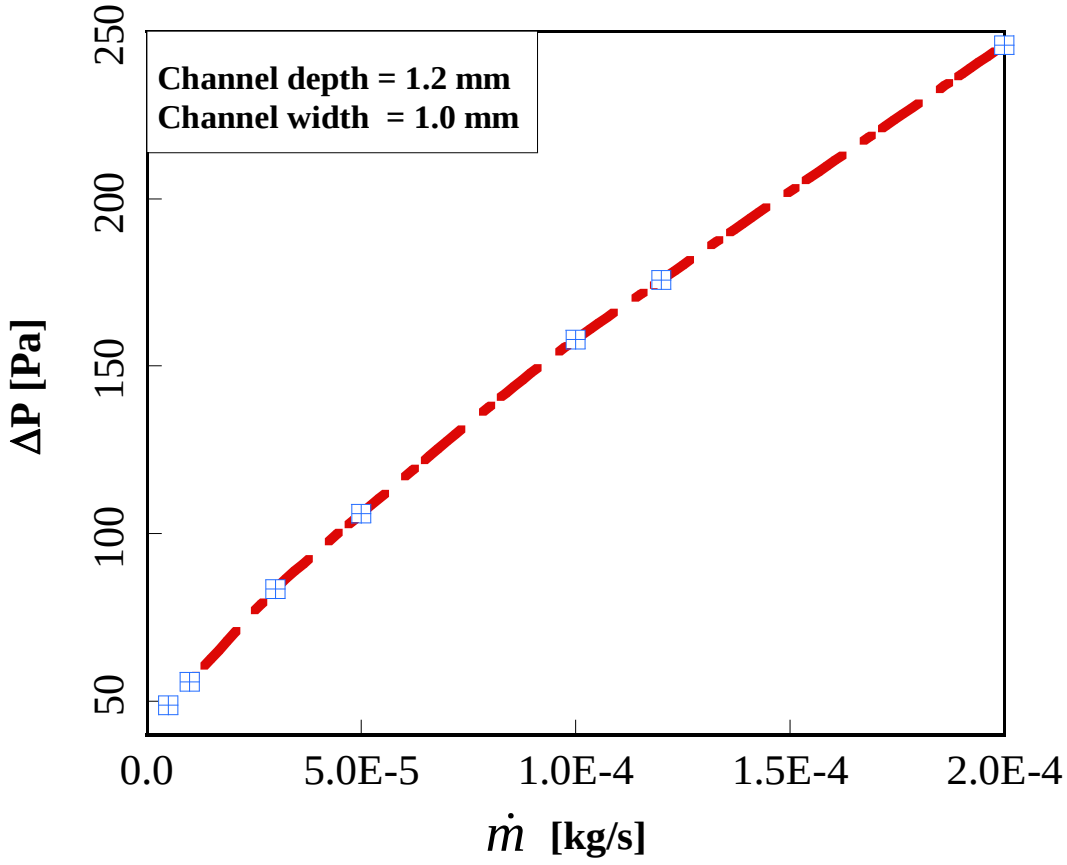

Figure 5 Pressure drop along the model flow channel at base operating conditions for a channel depth of 2.0 mm and width of 1.2 mm.

3.2 Effect of physical parameters on PEM fuel cell performance

Figure 6 illustrates the polarisation curves obtained from the model at several operating temperatures from 60 to 90 ^{o}C at stochiometry ratios of 1.2 and 2.0, respectively for the anode and the cathode**.** The curve indicates that the fuel cell performance increase with increase in temperature and is at optimum at temperatures of approximately 60 to 80 ^{o}C. This is consistent with literature [19,50]. The increase in the fuel cell performance with increase in temperature is attributable to an increase in gas diffusivity and membrane conductivity at higher operating temperatures.

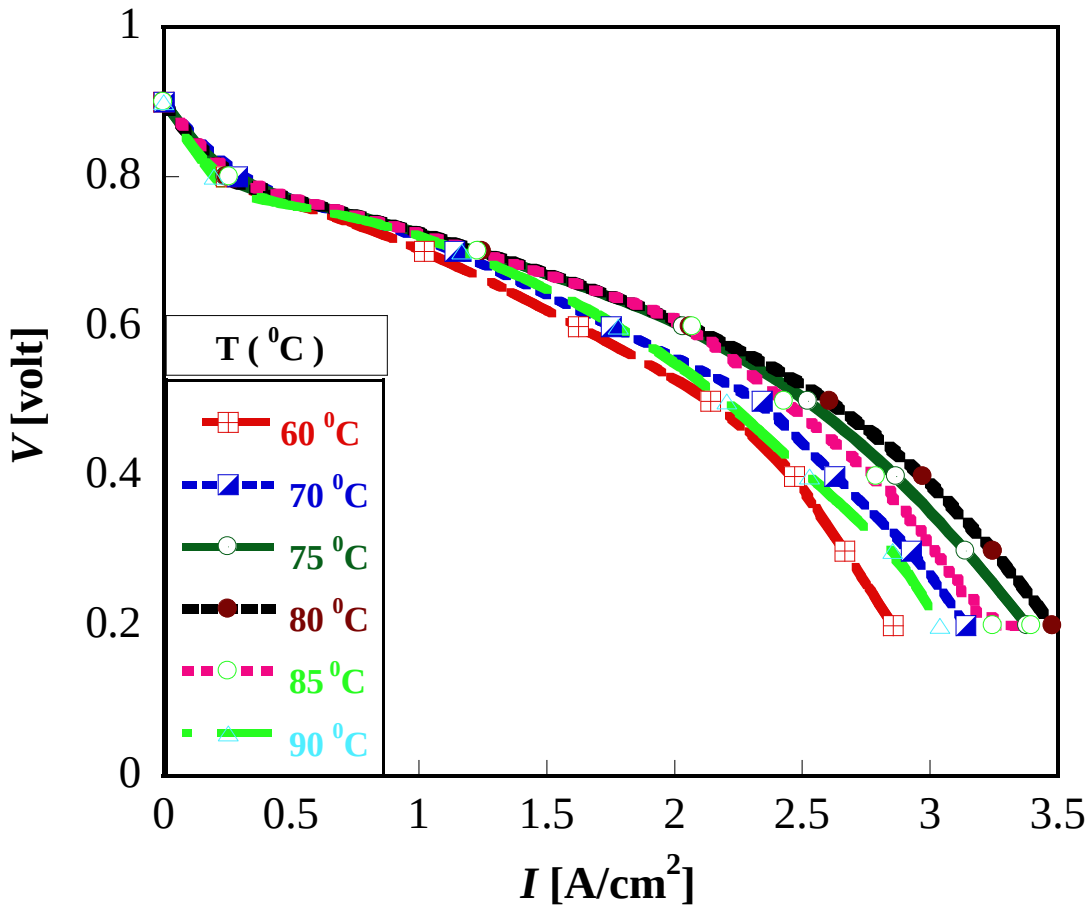

Figure 6 Effect of temperature on cell performance at base conditions.

The polarisation curves are also lower at 75 - 80 ^{o}C compared with 60 - 70 ^{o}C in the lower current density region, primarily due to the lower reaction rates resulting in low water content in the membrane. The condensation of water easily occurs at lower temperatures resulting in flooding and deteriorating the gas diffusivity in the catalyst layer and the gas diffusion layers. At temperatures beyond 80 ^{o}C the cell

performance declines, because membrane conductivity decreases at high temperatures due to the onset of reduction in relative humidity of reactant gases and water content in the membrane. Hence, the fuel cell performance is adversely affected at temperatures between 80 and 90 ^{o}C. Increasing the cell temperature beyond 80 ^{o}C result in higher levels of water loss in the cell until a critical temperature is attained where the evaporated water is greater than the amount of water being generated in the cell thereby resulting in total dry-out of the membrane. This could eventually lead to fuel cell failure. This model ascertains the fact that these fuel cells need to be operated at temperatures below 80 ^{o}C. A humidifier may be required if operation at higher temperatures is required but this adds to the capital and running costs of fuel cells.

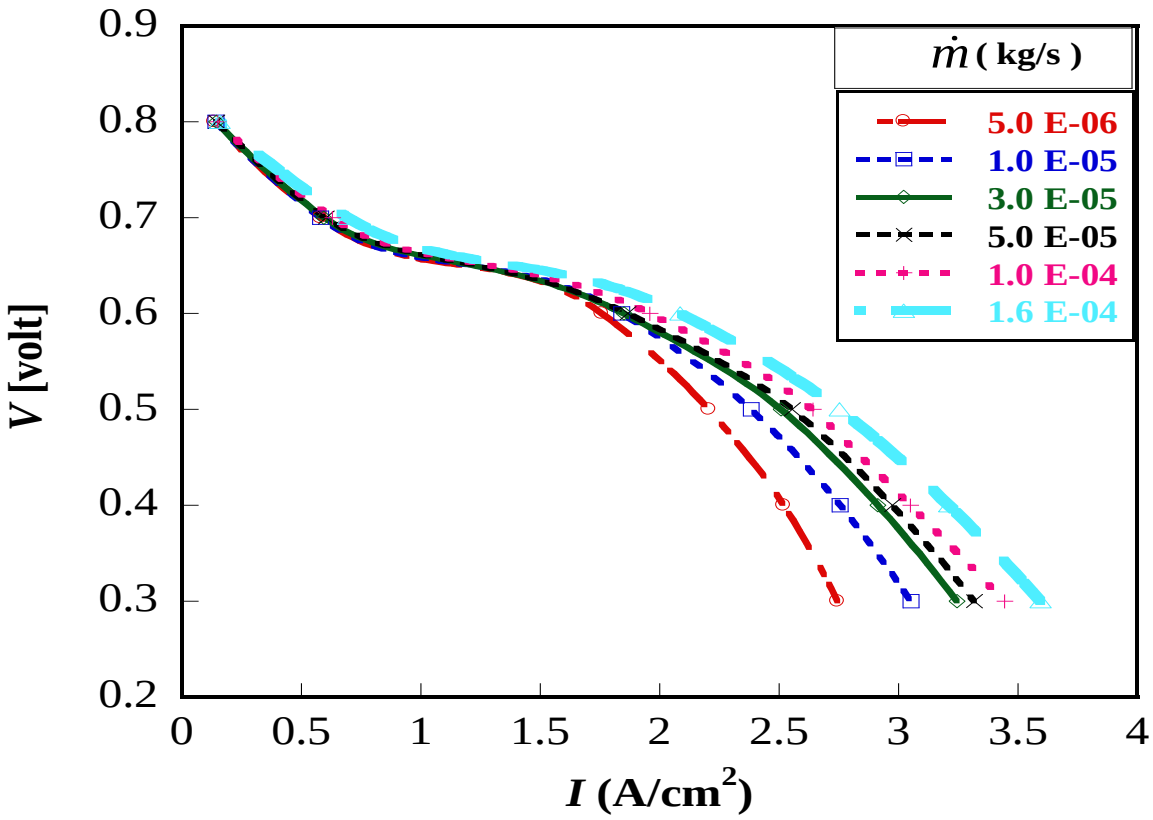

Figure 7 Effect of cathode gas flow rate on cell performance at base conditions.

Figure 7 shows the effect of changing the oxygen mass flow rate from 5.0E-06 to 1.6E-04 kg/s on the fuel cell performance. When the cathode gas mass flow rate is increased, the fuel cell performance is enhanced especially at lower operating fuel cell voltages. The reason is the increase in oxygen gas through the gas diffusion layer to the reaction sites, which increases the rate of reaction. At low operating voltages,

more liquid water is produced due to stronger electrochemical reaction rates, which is expected to reduce fuel cell performance. However, the high oxygen mass flow rates in the porous layer generate high shear forces, which aid the transport of liquid water downstream at the flow channel along the flow direction. The effect is minimal at high operating voltages as observed on the curves primarily due to low membrane humidification. Wang and Liu [51] obtained similar results in their experimental work on PEM fuel cell performance. This is because low amount of water presence occurs at these voltage levels due to slow reaction rates coupled with an increase in the oxygen gas supply resulting in reduced cell performance.

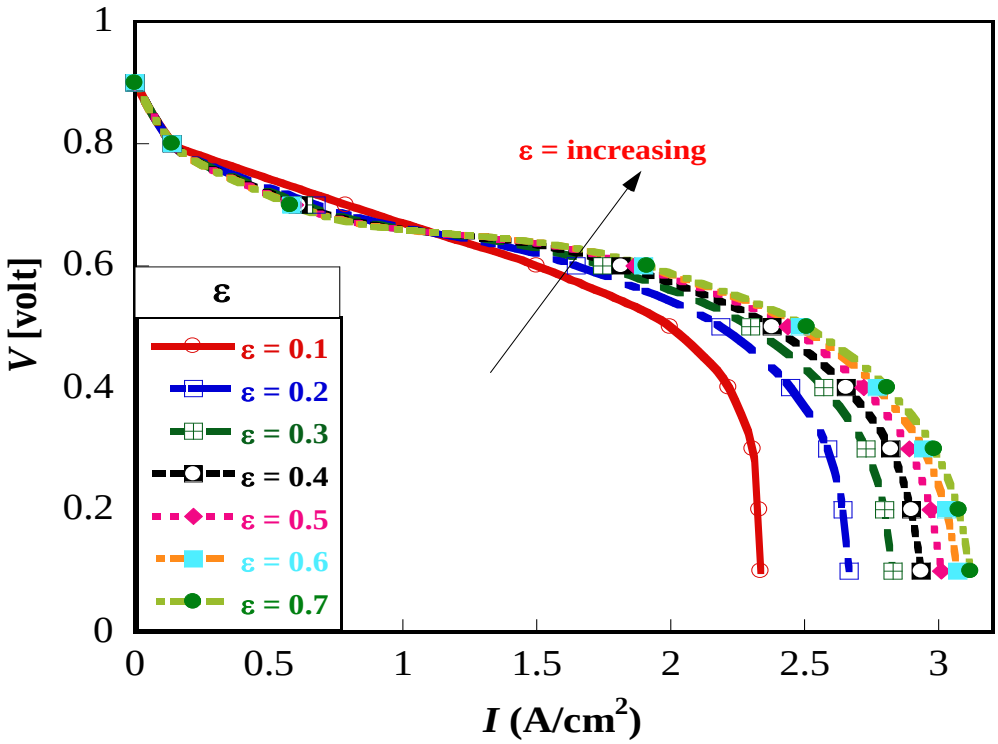

Figure 8 Effect of gas diffusion layer porosity on cell performance at base conditions.

The effect of the gas diffusion layer porosity on the performance of the PEM fuel cell is shown in Figure 8. The results show the fact that the effect of gas diffusion layer porosity on fuel cell performance is significant when the gas diffusion layer is in the low value region (0.1 to 0.4). Increasing the diffusion layer porosity size has an increasingly weaker effect on the performance. The gas diffusion layer porosity beyond 0.6 does not have a significant effect on the fuel cell polarisation curve. This observation is in agreement with optimisation work of Lin *et al.* [50]. They reported an optimum GDL porosity of 0.5913 for PEM fuel cell modeled in

their study. Therefore, maintaining porosity levels between 0.4 and 0.6 will be a reasonable value for the fuel cell if durability issues in the fuel cell structure are to be taken into consideration.

3.3 Effect of design parameters on PEM fuel cell performance

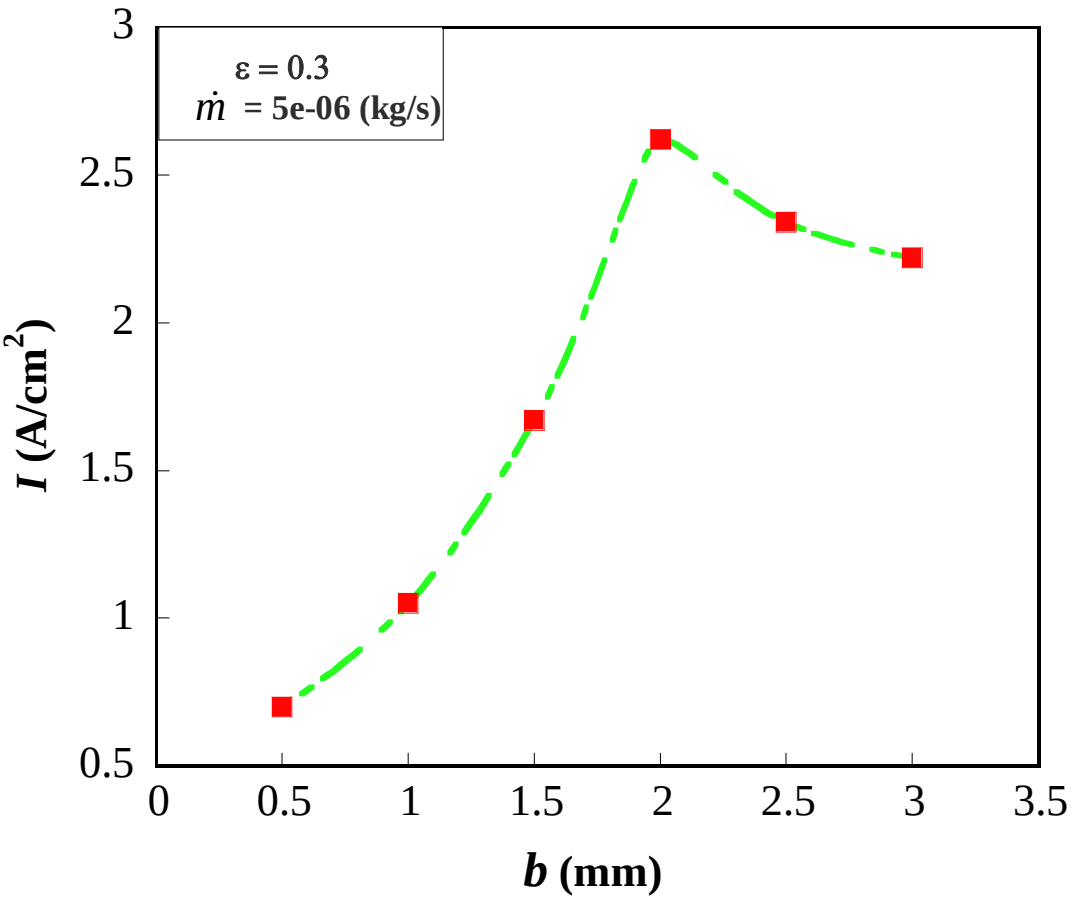

Figure 9 The cell current density at different channel depths at a cell potential of 0.3 V and a temperature 70 ^{0}C, and a mass flow rate of 5e-06 kg/s.

Simulations were performed for different sets of channel dimensions. Two different parameters which are channel width and channel depth were chosen for the study. Figure 9 illustrates the effect of channel depth on the fuel cell performance at a constant channel length. The optimal current density for the fuel cell was obtained at a channel depth of 2.0 mm (current density: 2.62 A/cm^2). A further increase in depth showed a decline in fuel cell performance.

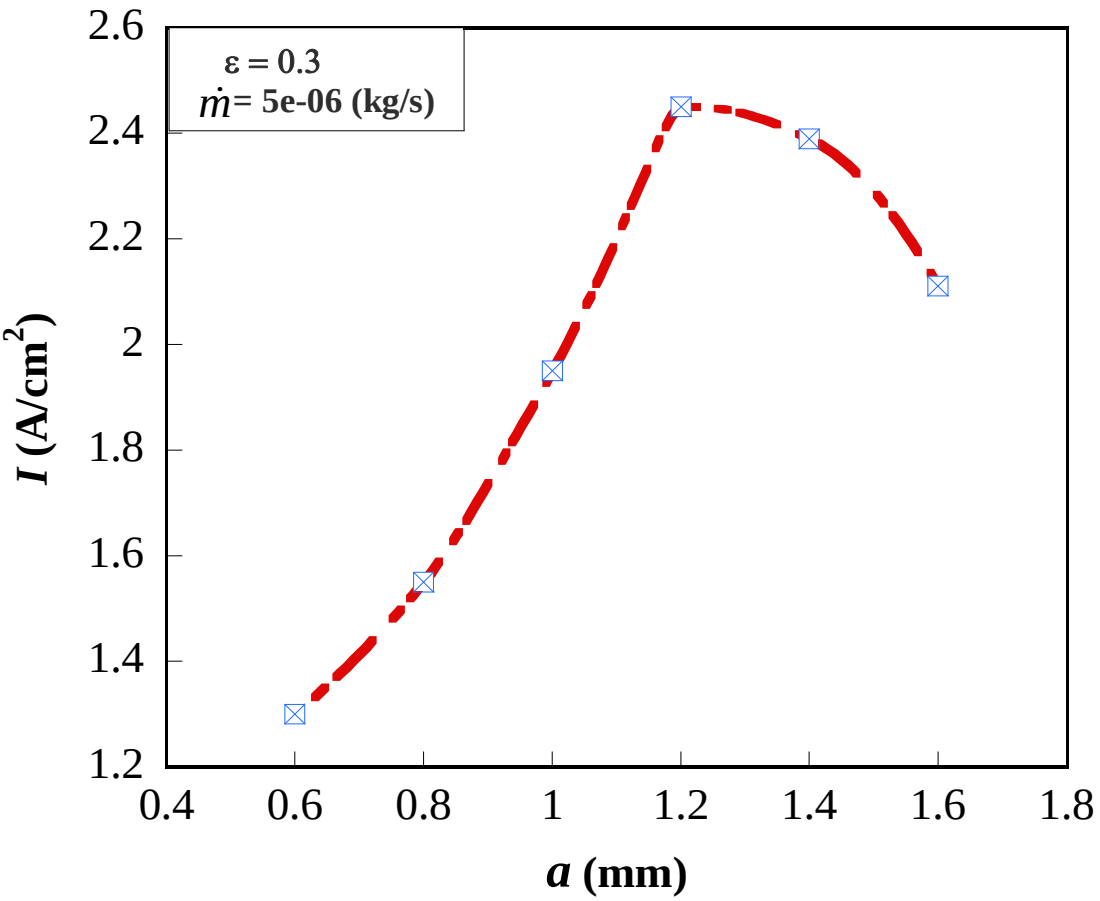

Figure 10 The cell current density at different channel widths at a cell potential of 0.3 V and a temperature of 70 ^{0}C.

Figure 10 shows the fuel cell performance for the six cases of channel widths considered. Performance increased gradually from case 1 (0.6 mm – current density: 1.30 A/cm^2) until an optimum was obtained at case 4 (1.2 mm – current density: 2.45 A/cm^2). Increasing the channel width beyond 1.2 mm showed a reduction in fuel cell performance. These results were consistent with those observed by other researchers. Watkins *et al.* [52] studied optimal dimension for cathode-side channels. They claimed that the most preferred ranges are 1.02 - 2.04 mm for channel depths and 1.14 - 1.4 mm for channel widths. Figures 9 and 10 suggest the existence of an optimal channel depth and width for the PEM fuel cell that will offer best system performance.

The effect of species flow orientation on the performance of the fuel cell was investigated for the base case. It was found that the direction of flow affects the performance of the fuel cell. The effect of co-flow and counterflow affect the fuel cell performance at different operating cell voltages. Figure 11 depicts the fuel cell

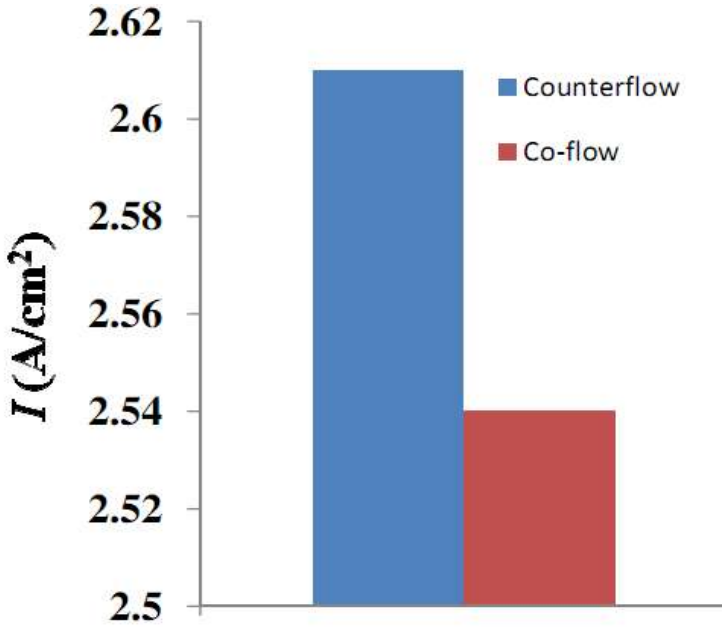

Figure 11 The cell **c**urrent density for counterflow orientation (2.61 A/cm^2) and co-flow orientation (2.54 A/cm^2) at base case conditions, for a channel depth of 2.0 mm and a channel width of 1.2 mm.

performance at the base case conditions and for a channel depth and width of 2.0 mm and 1.2 mm, respectively, for the counterflow and the co-flow orientations. Current densities of 2.61 A/cm^2 and 2.54 A/cm^2 were obtained for the counterflow and co-flow cases, respectively. Counterflow creates better performance for the fuel cell especially at higher current voltages.

Figures 12 shows the contours of mass fraction for hydrogen at the anode for counterflow (Figure 12a) and co-flow cases (Figure 12b), respectively. The contour shows that counterflow configuration allows more uniform distribution of the hydrogen species at the anode flow channel, which subsequently improves the performance of the fuel cell. The effective species distribution generally aids reaction on the membrane sites and this leads to increased current density.

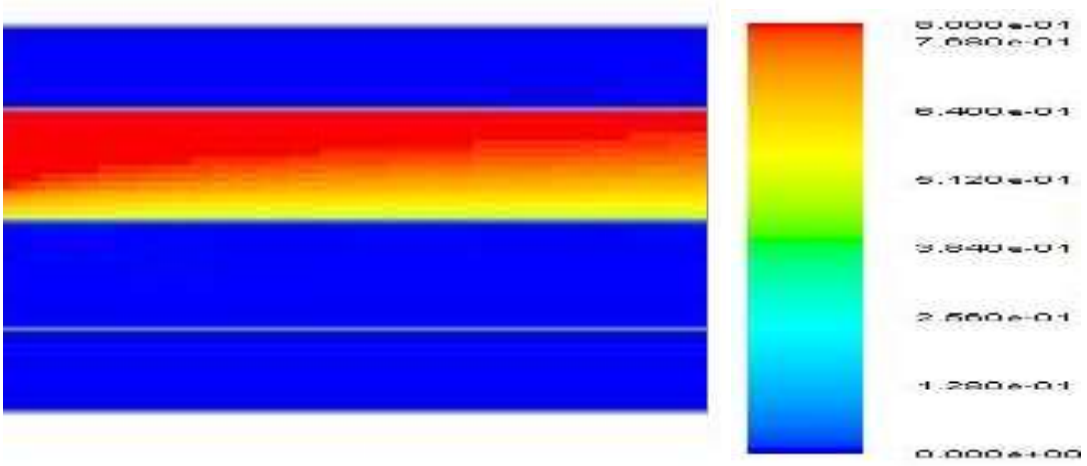

(a.) Counter flow

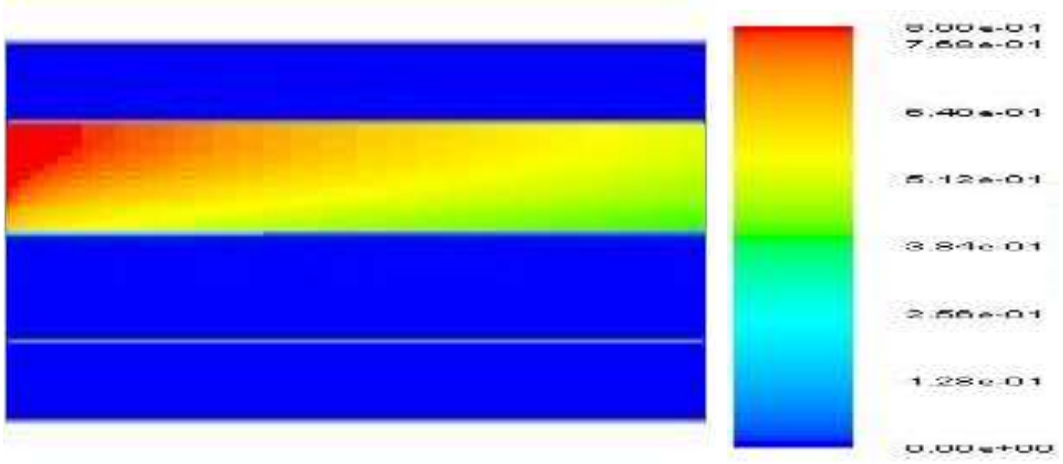

(b.) Co-flow

Figure 12 Contours of mass fraction of hydrogen at the anode for (a.) counterflow and (b.) co-flow cases at the base case operating conditions.

3.4 Optimal channel geometry

The results in section 3.3 (Figures 9 and 10) depicts the existence of an optimal channel depth and width for a PEM fuel cell system. The search for an optimal channel depth and width was carried out for the PEM fuel channel at varying GDL porosities. The first run of the simulation was carried out by fixing the cathode gas flow rate at 5e-06 kg/s, width of channel at 1.2 mm, cell operating voltage at 0.3 V and gas diffusion layer porosity at 0.2. The channel depth was then varied between 0.5 and 3.0 mm. An optimal channel depth, b_{opt} , was found for this configuration. The procedure was repeated for other values of gas diffusion layer porosities in the

range of $0.2 \leq \varepsilon \leq 0.6$ as shown in Figure 13, until an optimal channel depth, which corresponds with the maximum current density, was obtained at each value of the gas diffusion layer porosity.

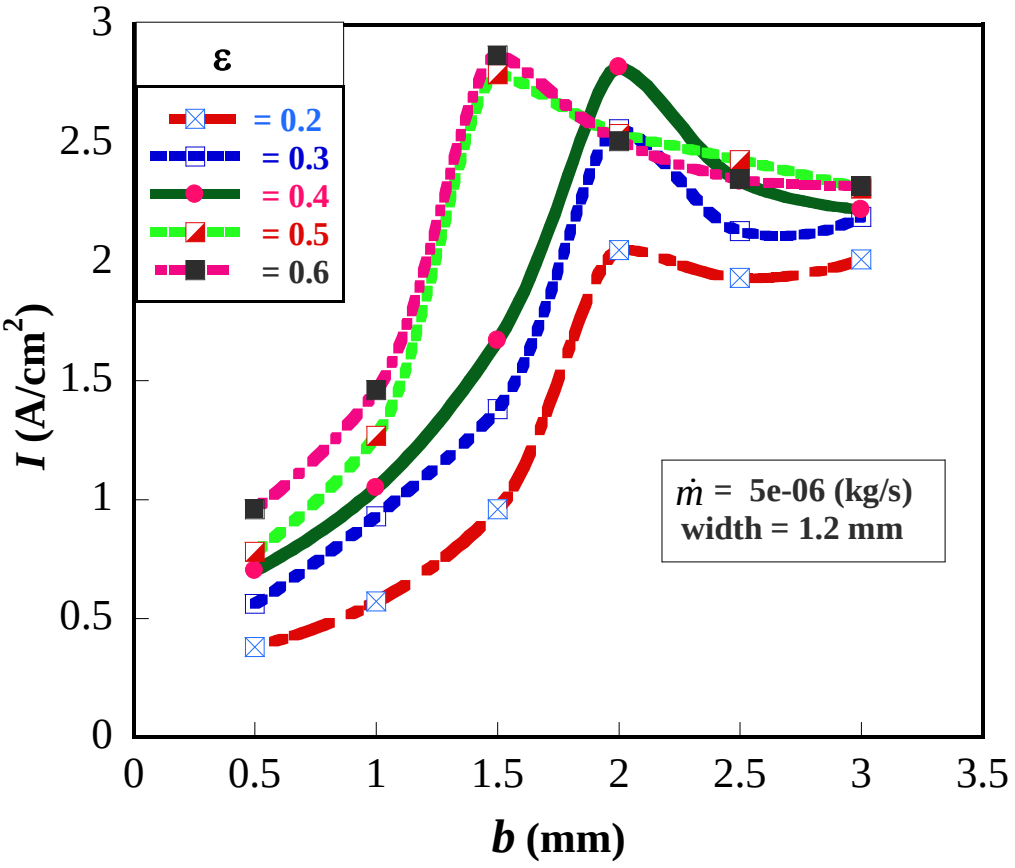

Figure 13 Effect of porosity and channel depth on the cell current density.

Figure 14 gives the optimum channel depth, b_{opt}, for different cathode gas mass flow rates for different gas diffusion layer porosities. The optimal channel depth decreases as the mass flow rate increases.

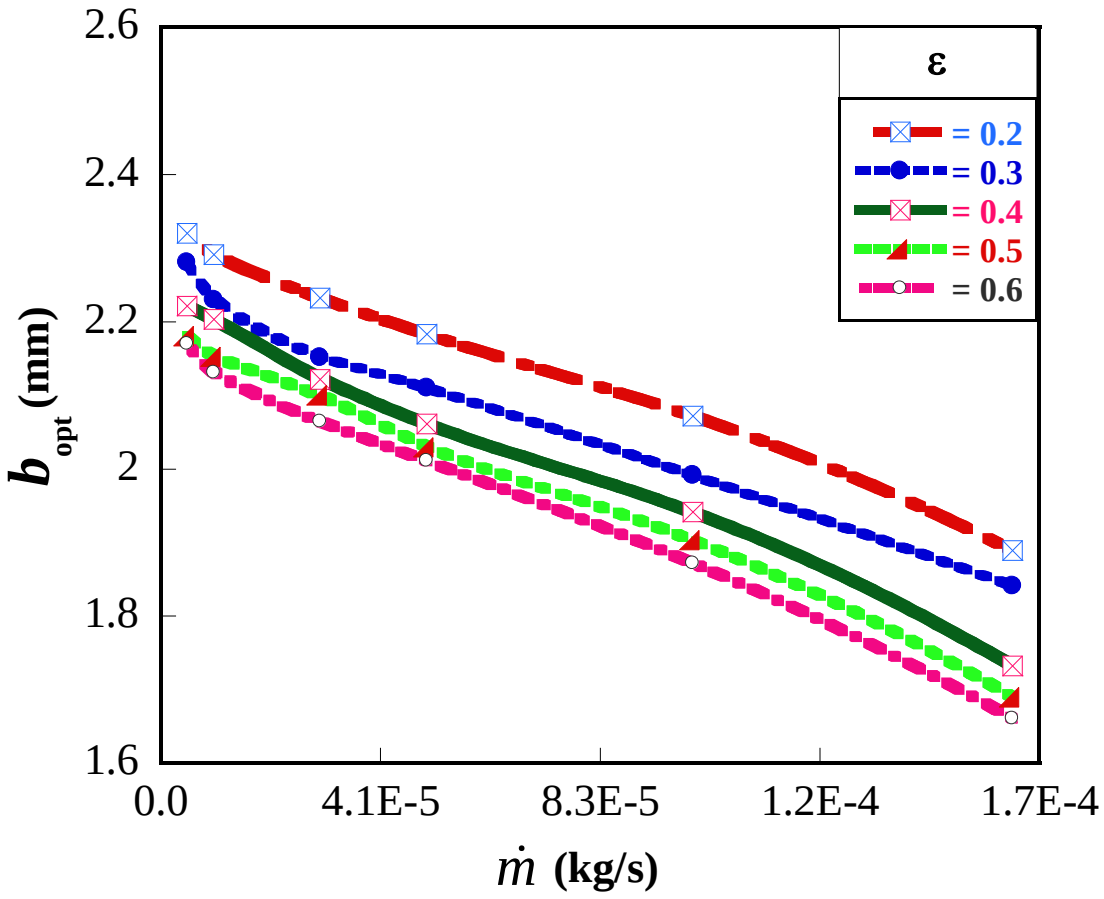

Figure 14 Optimum depths as a function of flow rate and gas diffusion layer porosity.

Figure 15 shows the behaviour of the maximum current density, I_{max}, with varying cathode gas mass flow rates. Each point of the figure depicts the result of a full optimisation with respect to channel depth. The graph shows that maximised current density increases as the mass flow rate of the reactant gas increases. In each case, there is an optimal channel depth that maximises the current density of the fuel cell.

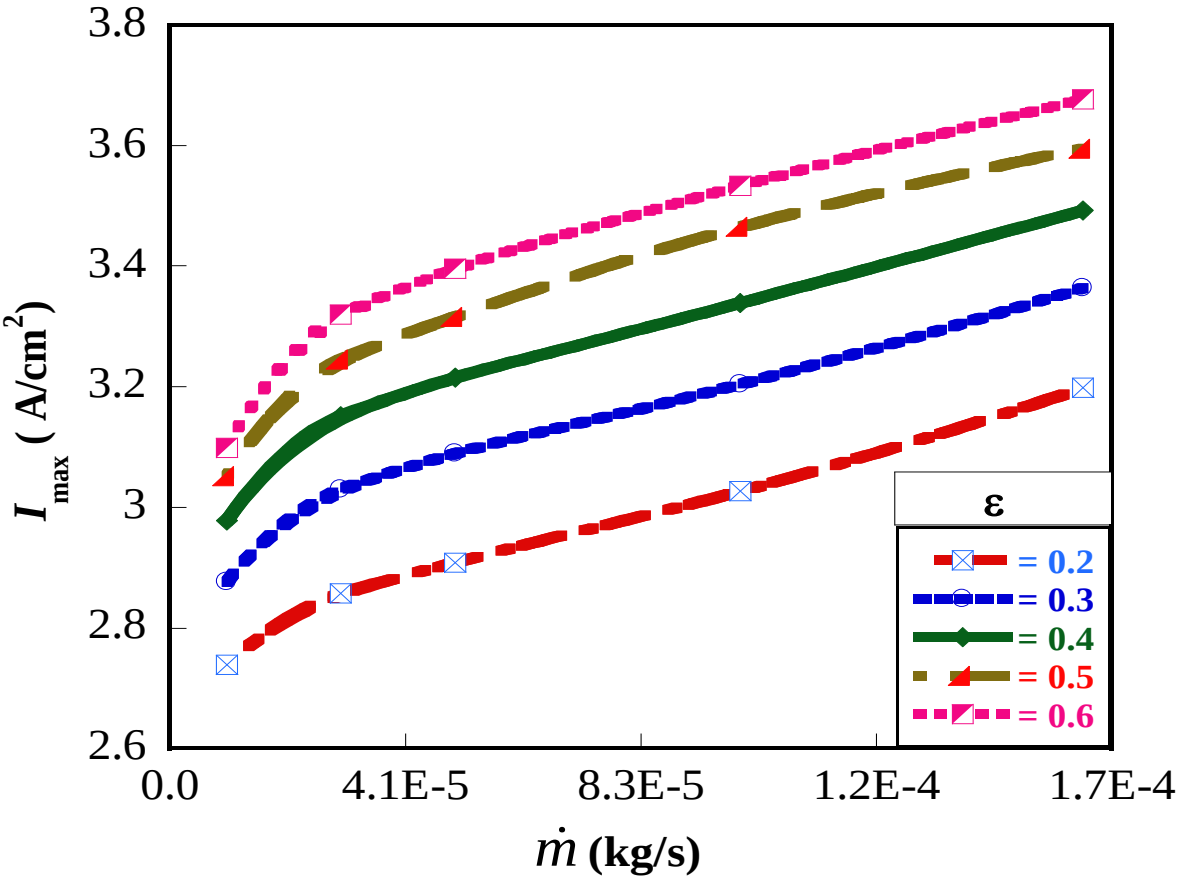

Figure 15 Effect of flow rate and gas diffusion layer porosity on the cell current density.

Similarly, the search for optimal channel widths, a_{opt}, corresponding to the maximum current density, I_{max}, was carried out as conducted for the channel depths. Figure 16 shows the current density value as a function of the channel widths for different values of gas diffusion layer porosities. The cathode gas mass flow rate and channel depth were initially fixed at 5e-06 kg/s and 2.0 mm, respectively.

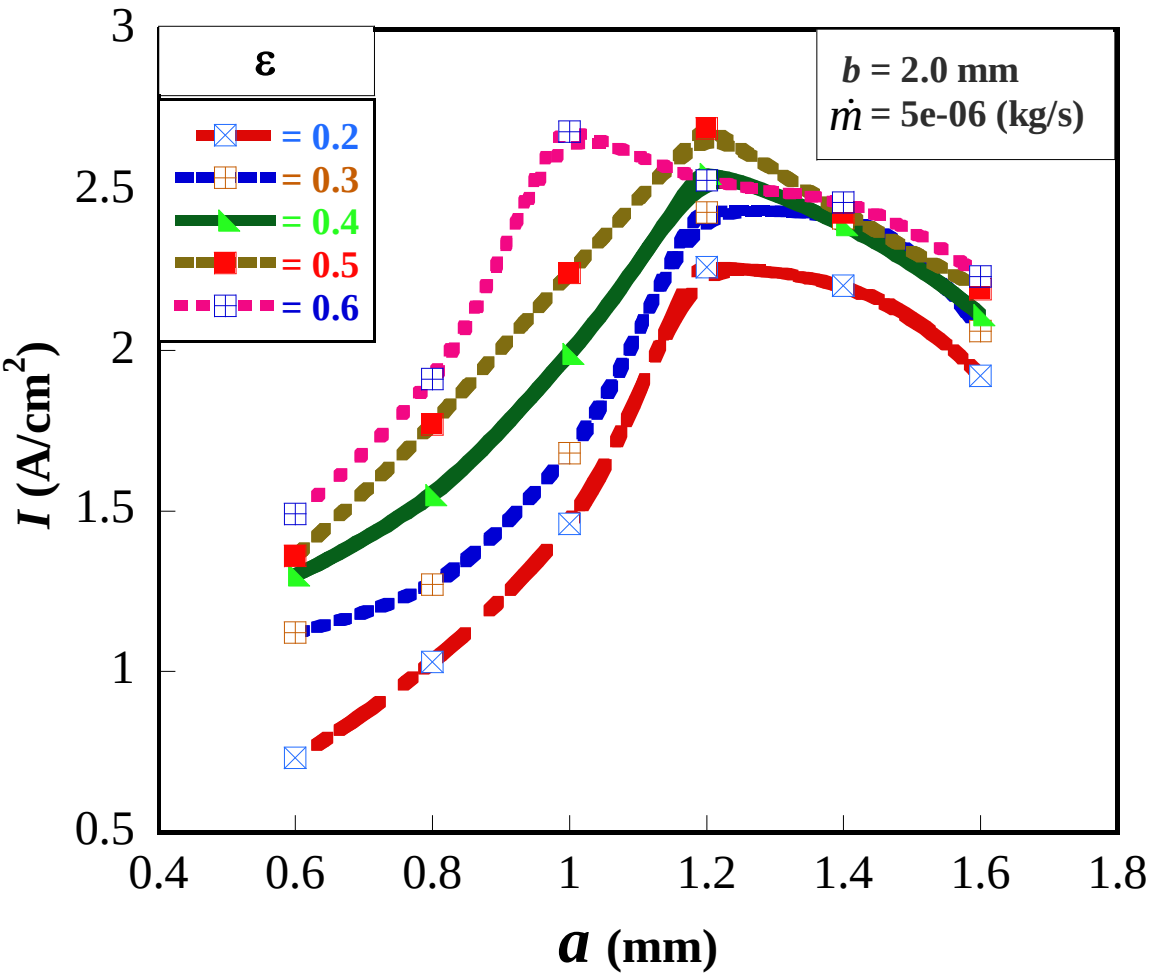

Figure 16 Effect of porosity and channel width on the cell current density.

Figure 17 depicts the optimal value of the channel width as a function of the cathode gas mass flow rate for each of the values of gas diffusion layer porosities ($0.2 \leq \varepsilon \leq 0.6$). The optimal channel widths, a_{opt}, from the figure decreases as the mass flow rate increases. The results obtained from Figures 14 and 17 both suggest that optimal channel depth and width decrease at increasing cathode gas mass flow rates. In designing PEM fuel cells it can be concluded that matching the fuel cell operating conditions and the gas fuel channel configuration is very important for optimum operation issues.

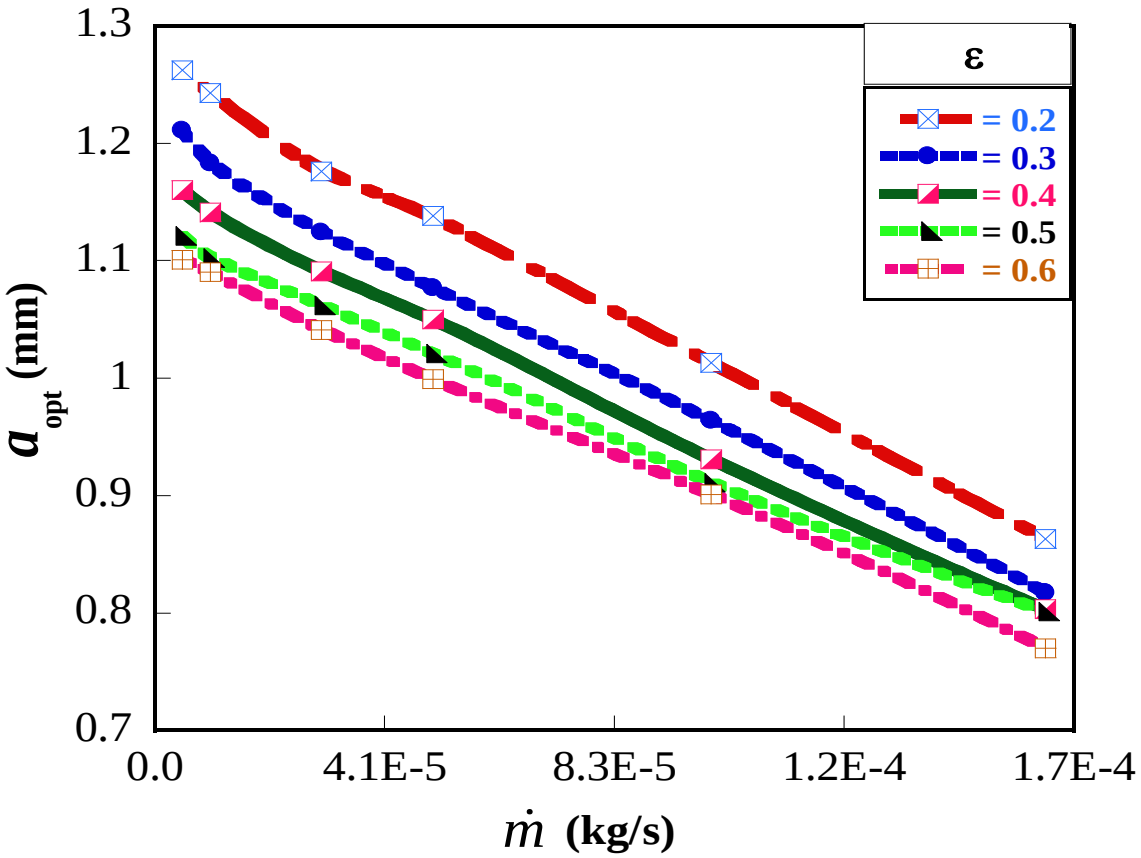

Figure 17 Optimum widths as a function of flow rate and gas diffusion layer porosity.

4. CONCLUSIONS

In this paper, a steady-state three-dimensional computational model was established to study the performance of a single channel proton exchange membrane fuel cell under varying operating conditions. The model prediction was validated by comparison with experimental data and was in good agreement. The numerical results provided detailed information on the effect of varying operating parameters of a single-channel fuel cell performance. Temperature, gas diffusion layer porosity, cathode gas mass flow rate and species flow orientation affect the performance of the fuel cell. In this work, the results show that fuel cell performance increases with increase in temperature from 60 to 80 ^{o}C. Further increase in temperature shows a decline in the fuel cell performance. The porosity of the GDL also affects the fuel cell performance. The porosity effects on fuel cell performance are more significant at porosity level of 0.1 to 0.4 than at porosity levels of 0.5 to 0.7. The effect of the

operating and design parameters on PEM fuel cell performance is also more dominant at low operating cell voltages than at higher operating fuel cell voltages. In addition, this study establishes the need to match the PEM fuel cell parameters such as porosity, species reactant mass flow rates and fuel gas channels geometry in the system design for maximum power output. Significant additional work is required for developed model implementation. The use of mathematical optimisation tool will improve the optimum model values obtained in this study. Most importantly, experimental work using data obtained from the present model as input design parameters is needed. Work is in progress that addresses these issues.

NOMENCLATURE

a	channel width (m)
A_c	cross-sectional area (m^2)
b	channel depth (m)
c_r	condensation rate constant
C	constant
D	gas diffusivity ($m^2\ s^{-1}$)
D_{eff}	effective diffusivity ($m^2\ s^{-1}$)
D_h	hydraulic diameter (m)
e	electrolyte
E_{OCV}	open-circuit voltage (V)
F	Faraday constant (96, 487 C mol^{-1})
f	friction factor
h	enthalpy (J kg^{-1})
h_L	enthalpy of condensation/vaporisation of water (J kg^{-1})
I	exchange current density (A m^{-2})
i_o	local current density (Am^{-2})
k	thermal conductivity (W $m^{-1}\ K^{-1}$)
L	channel length (m)
$\dot{m}$	channel mass flow rate (kg/s)
n	electron number
P	pressure (Pa)
P^*	wetted perimeter
P_c	capillary pressure (Pa)
r_w	water condensation rate (s^{-1})
R	universal gas constant (8.314 J $mol^{-1}\ K^{-1}$)
Re	Reynolds number
R_{ohm}	resistance of proton transfer through electrolyte membrane (Ωm^2)
S	liquid saturation or source term
S_h	volumetric heat source term
t	time (s)
T	temperature (K)
V	cell potential (V)

V_{avg}	mass-averaged velocity (m/s)
v	component of velocity (m/s)
x, y, z	coordinate (m)

Greek

Δ	difference operator
β	permeability (m^2)
ε	porosity
μ	fluid viscosity (kg m^{-1} s^{-1})
α_{an}	electrical transfer coefficient (anode)
α_{cat}	electrical transfer coefficient (cathode)
λ	membrane water content
κ	constant reaction parameter
η	over-potential (V)
Φ	phase potential function (V)
ρ	density (kg m^{-3})
τ	tortuosity

Subscripts

an	anode
avg	average
c	capillary
cat	cathode
eff	effective
l	liquid water
m	mass moment source
max	maximum
opt	optimum
px, py, pz	momentum source terms
react	electrochemical reaction
ref	reference value
s	electronic conductive solid matrix
sat	saturation
T	energy source term
w	liquid water source
v	vapor phase
x,y.z	components in the *x*-, *y*- and *z*- directions

CFD	computational fluid dynamics
GDL	gas diffusion layer
MEA	membrane electrode assembly
PEM	proton exchange membrane

ACKNOWLEDGEMENTS

The authors acknowledge the support of the Department of Mechanical and Aeronautical Engineering, University of Pretoria, the National Research Foundation and the Solar Hub between the University of Pretoria and Stellenbosch which is supported by the Department of Energy.

REFERENCES

[1] Rowe A, Li X. Mathematical modeling of proton exchange membrane fuel cells. *J. Power Sources* 2001; **102**:82-96.

[2] Hussain MM, Baschuk JJ, Li X, Dincer I. Thermodynamic analysis of a PEM fuel cell power system. *Int. J. Thermal Sciences* 2005; **44**:903-911.

[3] Jung HM, Lee WY, Park JS, Kim CS. Numerical analysis of a polymer electrolyte fuel cell. *Int. J. Hydrogen Energy* 2004; **29**:945-954.

[4] Du L, Jana SC. Highly conductive/graphite composites for bipolar plates in proton exchange membrane fuel cells. *J. Power Sources* 2007; **172**:734-741.

[5] Um S, Wang CY, Chen KS. Computational fluid dynamics modeling of proton exchange membrane fuel cells. *J. Electrochem. Soc.* 2000; **147**(12): 4485-4493.

[6] Bernardi DM. Water balance calculations for solid polymer electrolyte fuel cells. *J. Electrochem. Soc.* 1990; **137**(12):3344-3345.

[7] Bernardi DM, Verbrugge MW. Mathematical model of a gas diffusion electrode bonded to a polymer electrolyte. *AIChE J.* 1991; **37**(8):1151-1163.

[8] Springer TE, Zawodzinski TA, Gottesfeld S. Polymer electrolyte fuel cell model. *J. Electrochem. Soc.* 1991; **138**(8):2334-2342.

[9] Kazim A, Forges P, Liu HT. Effects of cathode operating conditions on performance of a PEM fuel cell with interdigitated flow fields. *International Journal of Energy Research* 2003; **27**:401-414.

[10] Kulikovsky AA. Two models of a PEFC: Semi-analytical vs numerical. *International Journal of Energy Research* 2005; **29**:1153-1165.

[11] Marr C, Li X. An engineering model of proton exchange membrane fuel cell performance. *ARI* 1998; **50**:190-200.

[12] Chen KS, Hickner MA, Noble DR. Simplified models for predicting the onset of liquid water droplet instability at the gas diffusion layer/gas flow channel interface. *International Journal of Energy Research* 2005; **29**:1113-1132.

[13] Dutta S, Shimpalee S, Van Zee JW. Numerical prediction of mass

exchange between cathode and anode channels in a PEM fuel cell. *Int. J. Heat Mass Transfer* 2001; **44**:2029-2042.

[14] Yuan W, Tang Y, Pan M, Li Z, Tang B. Model prediction of effects of operating parameters on proton exchange membrane fuel cell performance. *Renewable Energy* 2010; **35**:656-666.

[15] Hontanon E, Escudero MJ, Bautista C, Garcia-Ybarra PL, Daza L. Optimization of flow-field in polymer electrolyte membrane fuel cells using computational fluid dynamics techniques. *J. Power Sources* 2000; **86**:363-368.

[16] Wang XD, Duan YY, Yan WM. Numerical study of cell performance and local Transport phenomena in PEM fuel cells with various flow channel area ratios. *J. Power Sources* 2007; **172**:265-277.

[17] Sinha PK, Wang C-Y, Beuscher U. Effect of flow field design on the performance of elevated-temperature polymer electrolyte fuel cells. *International Journal of Energy Research* 2007; **31**:390-411.

[18] Golpaygan A, Sarchami A, Ashgriz N. Three-dimensional multiphase flow model to study channel flow dynamics of PEM fuel cells. *International Journal of Energy Research* 2010; DOI:**10**.1002/er.1775.

[19] Yan Q, Toghiani H, Causey H. Steady state and dynamic performance of proton exchange membrane fuel cells (PEMFCs) under various operating conditions and load changes. *J. Power Sources* 2006; **161**:492-502.

[20] Vargas JVC, Bejan A. Thermodynamic optimization of internal structure in a fuel cell. *International Journal of Energy Research* 2004; **28**:319-339.

[21] Zhang Z, Jia Li. Parametric study of the porous cathode in the PEM fuel cell. *International Journal of Energy Research* 2009; **33**:52-61.

[22] Zamel N, Li X. A parametric study of multi-phase and multi-species transport in in the cathode of PEM fuel cells. *International Journal of Energy Research* 2008; **32**:698-721.

[23] Huang W, Zhou B, Sobiesiak A. Along-channel mathematical modelling for proton exchange membrane fuel cells. *International Journal of Energy Research* 2005; **29**:1051-1071.

[24] Cheddie DF, Munroe NDH. A two-phase model of an intermediate temperature PEM fuel cell. *Int. J. Hydrogen Energy* 2007; **32**:832-841.

[25] Springer TE, Wilson MS, Gottesfeld S. Modeling and experimental diagnostics in polymer electrolyte fuel cells. *J. Electrochem. Soc*. 1993; **140**(12):3513-3526.

[26] Mench MM, Wang CY, Ishikawa M. In-situ current distribution

measurements in polymer electrolyte fuel cells. *J. Electrochem. Soc*. 2003; **150**(8):A1052-A1059.

[27] Weizhong L, Zhixiang L, Cheng W, Zongqiang M, Milin Z. The effects of pinholes on proton exchange membrane fuel cell performance. *International Journal of Energy Research* 2010; **35**:24-30.

[28] Ferng YM, Su A, Lu SM. Experiment and simulation investigations for effects of flow channel patterns on the PEMFC performance. *International Journal of Energy Research* 2008; **32**:12-23.

[29] Inoue G, Matsukuma Y, Minemoto M. Effect of gas channel depth on current density distribution of polymer electrolyte fuel cell by numerical analysis including gas flow through gas diffusion layer. *J. Power Sources* 2006; **157**:136-152.

[30] Liu X, Guo H, Ma C. Water flooding and pressure drop characteristics in flow channels of proton exchange membrane fuel cells. *Electrochim. Acta* 2007; **52**:3607-3614.

[31] Rodatz P, Buechi F, Onder C, Guzzella L. Operational aspects of a large PEFC stack under practical conditions. *J. Power Sources* 2004; **128**:208-217.

[32] Maharudrayya S, Jayanti S, Deshpande AP. Pressure drop and flow distribution in multiple parallel-channel configurations used in proton-exchange membrane fuel cell stacks. *J. Power Sources* 2006; **157**:358-367.

[33] Ahmed DH, Sung HJ. Effects of channel geometrical configuration and shoulder width on PEMFC performance at high current density. *J. Power Sources* 2006; **162**:327-339.

[34] Cheng CH, Lin HH, Lai G. Design for geometric parameters of PEM fuel cell by integrating computational fluid dynamics code with optimisation method. *J. Power Sources* 2007; **165**:803-813.

[35] Ansys *Fluent® 12.0 Users Guide Documentation*, Ansys Inc., Southpointe, SAS, 2009.

[36] Nguyen TV. Modeling two-phase flow in the porous electrodes of proton exchange membrane fuel cells using the interdigitated flow fields. *Tutorials in Electrochemical Engineering Mathematical Modeling* 1999; **99(14)**:222-241.

[37] Nam JH, Karviany M. Effective diffusivity and water-saturation distribution in Single-and two-layer PEMFC diffusion medium. *Int. J. Heat Mass Transfer* 2003; **46**:4595-4611.

[38] Kim YB. Study on the effect of humidity and stoichiometry on the water

saturation of PEM fuel cells. *International Journal of Energy Research* 2011; DOI:**10**.1002/er.1845.

[39] Maharudrayya S, Jayanti S, Deshpande AP. Pressure losses in laminar flow through serpentine channels in fuel cell stacks. *J. Power Sources* 2004; **138**:1-13.

[40] White FM. *Fluid Mechanics*. McGraw Hill: New York, 1986.

[41] White FM. *Viscous Fluid Flow*. McGraw Hill: New York, 1991; 119-122.

[42] Mench MM. *Fuel Cell Engines*. John Wiley & Sons: New Jersey, 2008.

[43] AIAA. Guide for the verification and validation of computational fluid dynamics simulations; AIAA **G-077**-1998, 1998.

[44] ASME Editorial Board. Journal of heat transfer editorial policy statement on numerical accuracy. *ASME Journal of Heat Transfer* 1994; **116**:797-798.

[45] Pantakar SV. *Numerical Heat Transfer and Fluid Flow*. Hemisphere Publishing Corp., New York, 1980.

[46] Tao WQ, Min CH, Liu XL, He YL, Yin BH, Jiang W. Parameter sensitivity examination and discussion of PEM fuel cell simulation model validation Part I. Current status of modeling research and model development. *J. Power Sources* 2006; **160**:359-373.

[47] Wang L, Husar A, Zhou T, Liu H. A parametric study of PEM fuel cell performances. *Int. J. Hydrogen Energy* 2003; **28**:1263-1272.

[48] Berning T, Djilali N. *J. Electrochem Soc*. 2003; **150**(12):A1598-A1607.

[49] Labaek J, Bang M, Kaer SK. Flow and pressure distribution in fuel cell manifolds. *ASME J. Fuel Cell Sci. Technology* 2010; **7**/061001-1.

[50] Lin HH, Cheng CH, Soong CY, Chen F, Yan WM. Optimisation of key parameters in the proton exchange membrane fuel cell. *J. Power Sources* 2006; **162**:246-254.

[51] Wang L, Liu H. Performance studies of PEM fuel cells with interdigitated flow fields. *J. Power Sources* 2004; **134**:185-196.

[52] Watkins DS, Dircks KW, Epp DG. Novel fuel cell fluid flow field plate. *US Patent* 4988583; 1991.